SUPPORTING INFORMATION

Solution-Based Synthesis and Processing of Sn- and Bi-Doped Cu$_3$SbSe$_4$ Nanocrystals, Nanomaterials and Ring-Shaped Thermoelectric Generators

Yu Liu,[a] Gregorio García,[b,c] Silvia Ortega,[a,d] Doris Cadavid,*[a] Pablo Palacios,[b,e] Jinyu Lu,[c] Maria Ibáñez,[f,g] Lili Xi,[h] Jonathan De Roo,[l,j] Antonio M. López,[k] Sara Martí-Sánchez,[l] Ignasi Cabezas,[d,k] María de la Mata,[l] Zhishan Luo,[a] Chaochao Dun,[m] Oleksandr Dobrozhan,[a] David. L. Carroll,[m] Wenqing Zhang,[h] José Martins,[j] Maksym V. Kovalenko,[f,g] Jordi Arbiol,[l,n] German Noriega,[d] Jiming Song,*[o] Perla Wahnón*[b,c] and Andreu Cabot*[a,n]

a. Catalonia Institute for Energy Research - IREC, 08930 Sant Adrià de Besòs, Barcelona, Spain *email: dcadavid@irec.cat, acabot@irec.cat
b. Instituto de Energía Solar, ETSI Telecomunicación, Universidad Politécnica de Madrid, 28040, Madrid, Spain. *email: perla@etsit.upm.es
c. Departamento de Tecnología Fotónica y Bioingeniería, ETSI Telecomunicación, Ciudad Universitaria, s/n, 28040 Madrid, Spain.
d. Cidete Ingenieros S.L. Anselm Clavé 98, 08800 Vilanova i la Geltrú, Spain
e. Departamento de Física aplicada a las Ingenierías Aeronáutica y Naval. ETSI Aeronáutica y del Espacio, Pz. Cardenal Cisneros, 3, 28040 Madrid, Spain.
f. Institute of Inorganic Chemistry, Department of Chemistry and Applied Biosciences, ETH Zürich, CH-8093, Switzerland
g. Empa-Swiss Federal Laboratories for Materials Science and Technology, Dübendorf, CH-8600, Switzerland
h. Materials Genome Institute, Shanghai University, Shanghai 200444, China
i. Department of Inorganic and Physical Chemistry, Ghent University, B-9000 Ghent, Belgium
j. Department of Organic and Marcromolecular Chemistry, Ghent University, B-9000 Ghent, Belgium
k. Departament d'Enginyeria Electrònica, Universitat Politècnica de Catalunya, EPSEVG, 08800 Vilanova i la Geltrú, Barcelona, Spain
l. Catalan Institute of Nanoscience and Nanotechnology (ICN2), CSIC and The Barcelona Institute of Science and Technology (BIST), Campus UAB, Bellaterra, 08193 Barcelona, Spain
m. Center for Nanotechnology and Molecular Materials Wake Forest University, 501 Deacon Blvd. Winston Salem NC 27109 USA
n. ICREA, Pg. Lluis Companys 23, 08010 Barcelona, Spain
o. School of Chemistry & Chemical Engineering, Anhui University, Hefei, Anhui, 230601, P. R. China *email: jiming@ahu.edu.cn

Contents

1. SEM and HRTEM

Figure S1. (a) Usual yield of CASe NCs obtained from one large-scale synthesis. (b) SEM image of CASe NCs after ligand exchange. Inset shows the stable, dark-green dispersion in chloroform formed by the NCs before ligand exchange.
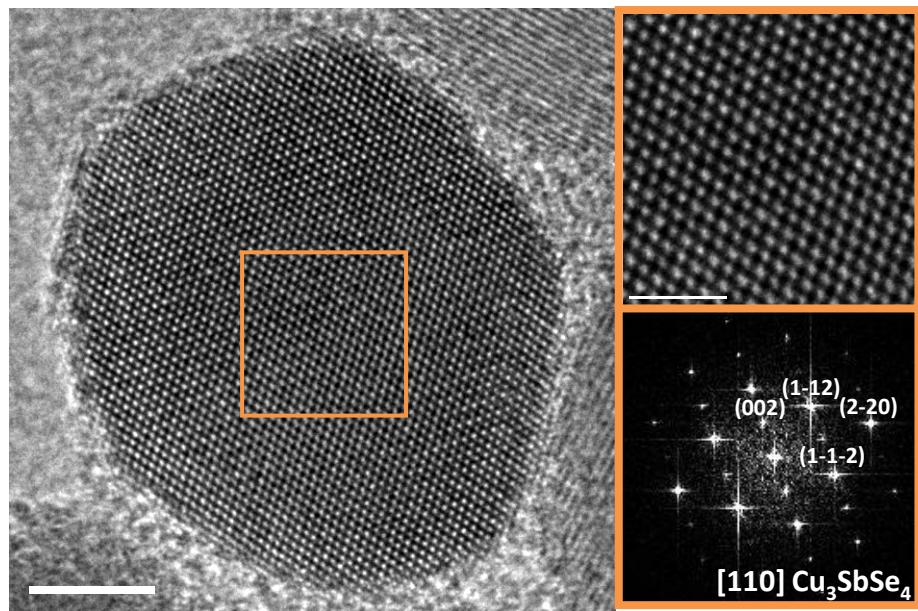

Figure S2. HRTEM image of a single CASe NC. On the right, detail of the squared regions and its respective power spectrum fitting showing the CASe tetragonal phase.

2. Crystal structure

Table S1. Summary of the peaks simulated for tetragonal CASe. (Crystal data: JCPDS No. 85-0003, Formula CASe, Crystal system Tetragonal, Space group $I\bar{4}2m$ (No. 121), Unit cell dimensions a = b = 5.6609 Å and c =11.280 Å).

hkl	d-spacing/ Å	2θ/deg	hkl	d-spacing/ Å	2θ/deg
101	5.0595	17.514	204	1.9977	45.360
110	4.0028	22.190	312	1.7062	53.675
112	3.2642	27.299	116	1.7016	53.831
103	3.1320	28.475	400	1.4152	65.953
202	2.5297	35.456	008	1.4100	66.229
211	2.4701	36.340	332	1.2984	72.775
114	2.3053	39.040	316	1.2964	72.908
105	2.0957	43.130	424	1.1548	83.677
220	2.0014	45.272	228	1.1526	83.867

3. Potential secondary phases
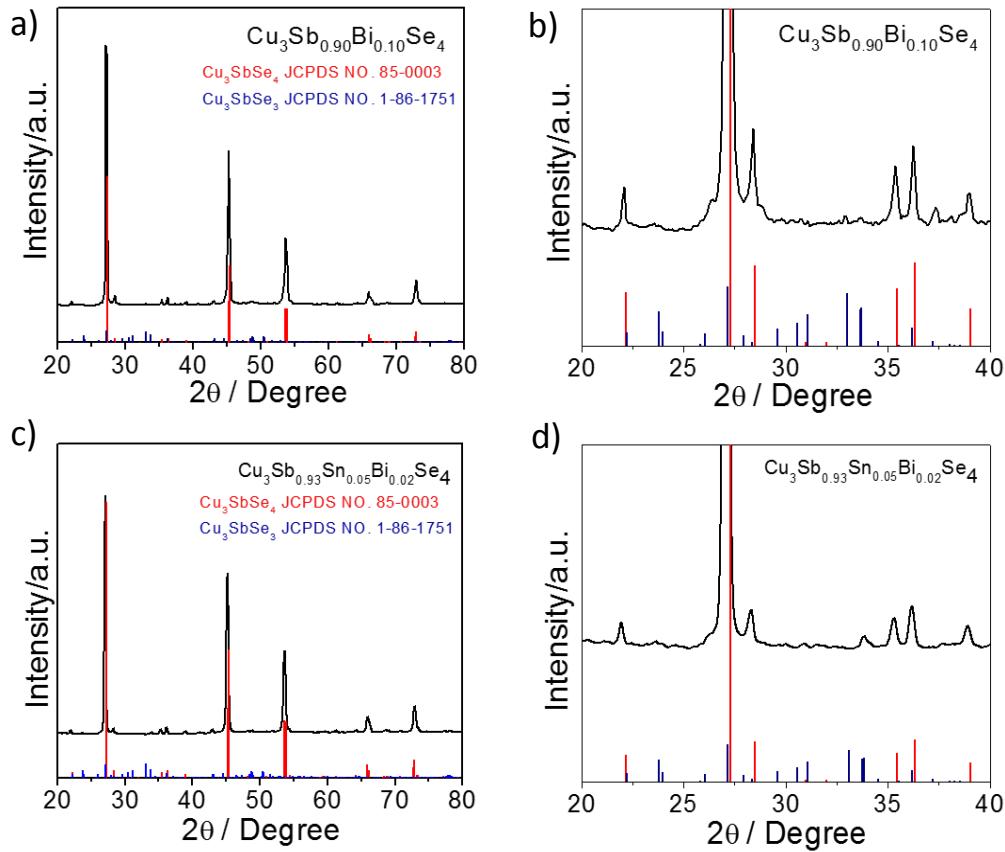
**Figure S3.** XRD patterns (a,c) and detail of the (112) peaks between 20º and 40º 2θ values (b,d) of $Cu_3Sb_{0.90}Bi_{0.10}Se_4$ (a,b) and $Cu_3Sb_{0.93}Sn_{0.05}Bi_{0.02}Se_4$ (c,d) pellets. Red vertical lines correspond to the reference literature data for Cu_3SbSe_4, JCPDS NO. 85-0003. Blue vertical lines correspond to Cu_3SbSe_3, JCPDS NO. 1-86-1751.

4. CASe NC composition
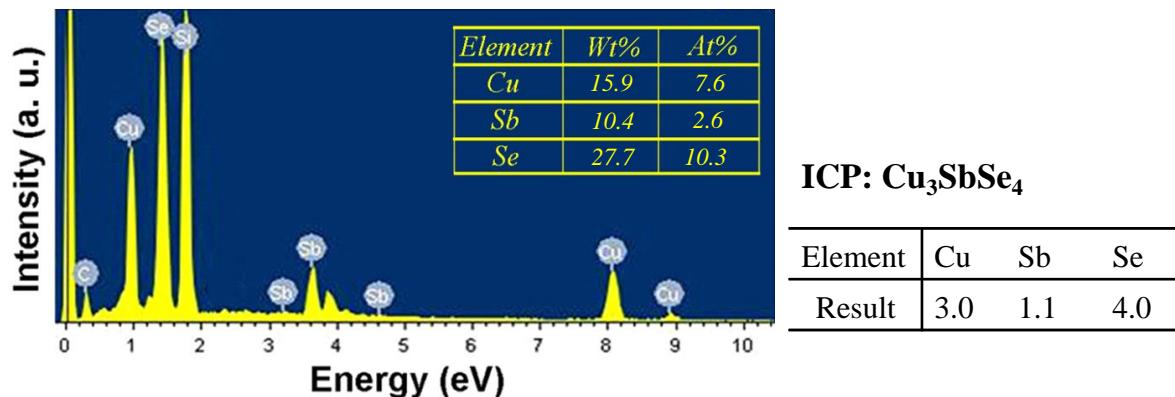
Figure S4. Left: EDX spectrum of CASe NCs and quantitative analysis of the as-synthesized CASe NCs showing a composition consistent with stoichiometric Cu_3SbSe_4. Right: Results of the ICP analysis of CASe NCs showing a composition of $Cu_{3.0}Sb_{1.1}Se_{4.0}$.
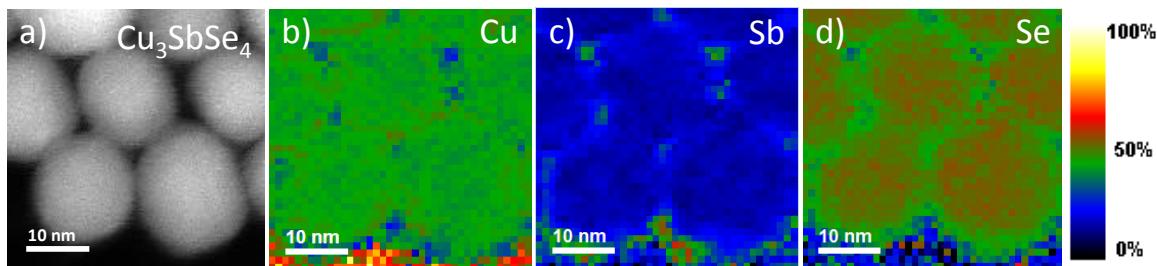

Figure S5. (a) HAADF-STEM image of CASe NCs. (b-d) relative atomic composition of Sb, Cu and Se.

5. XPS characterization

XPS analysis was performed to investigate the chemical state of elements within CASe NCs. The survey scan is shown in Figure S6a. High-resolution spectra of Cu 2p, Sb 3d, and Se 3d are shown in figure 6b, c, and d, respectively. All spectra were shifted to locate the C1s peak at 284.6 eV, correcting in this way potential charging effects. The two peaks in the Cu 2p spectrum appear at 932.1 eV ($2p_{3/2}$) and 951.9 eV ($2p_{1/2}$), consistent with the standard separation of 19.8 eV and indicative of Cu (I) (Figure S5b).[1, 2] In addition, we exclude the presence of Cu^{2+} because the Cu $2p_{3/2}$ satellite peak of Cu (II) (936 eV and 942 eV) did not appear in the spectrum.[3]

Figure S6c displays the Sb 3d peaks at surprisingly low binding energies, 528.7 eV and 538.1 eV, which could be related to the observed Se-poor surface of the NCs. Nevertheless, there has been debate on the specific valence number of Sb in CASe, both Sb^{5+} and Sb^{3+} have been suggested.[4-6] In this compound, the Sb 5s bands are quite narrow ~0.5 eV and typically located approximately at 529.5 eV ($3d_{5/2}$) and 538.9 eV ($3d_{3/2}$), while the Sb p bands are above the Fermi level.[4]

Figure S6d shows the Se $3d_{5/2}$ peak at 54.75 eV, indicating Se with a valence of Se^{2-}. In the inset of Figure S6d, we observe the Se 3p core located at 161.1 eV ($3p_{3/2}$) and 166.8 eV ($3p_{1/2}$) with a peak separation of 5.7 eV, which are in good agreement with values reported previously for Se $3p_{3/2}$ and $3p_{1/2}$, respectively. [1, 7]
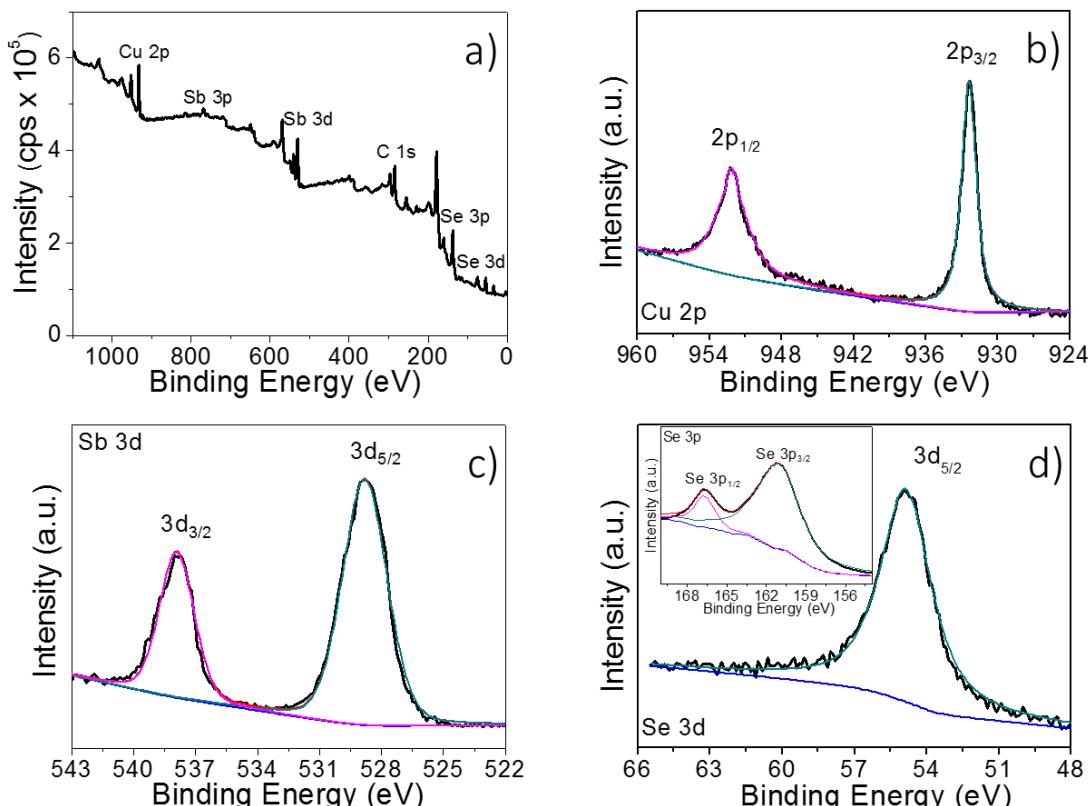
Figure S6. XPS spectrum of the obtained CASe NCs: (a) survey spectrum of CASe, and high resolution spectrum of (b) Cu 2p, (c) Sb 3d, and (d) Se 3d.

Figure S7 shows the XPS spectra of $Cu_3Sb_{0.90}Bi_{0.10}Se_4$ NCs. Figure S7e shows the high resolution spectrum of the Bi 4f region. The Bi $4f_{5/2}$ and $4f_{7/2}$ peaks exist at binding energies of 166.2 eV and 161.0 eV, respectively. These values are slightly above those generally reported for Bi^{3+} compounds such as Bi_2Se_3[8-10] and Bi_2O_3.[11] However, Bi^{5+} is a very strong oxidizer with a very high reduction potential (Bi^{3+}/Bi^{5+} E = 2V), which makes it extremely improvable to be found within CASe, especially taking into account Bi was introduced as Bi^{3+}.

The high resolution XPS spectrum of the Bi 4f region obtained from the $Cu_3Sb_{0.88}Sn_{0.10}Bi_{0.02}Se_4$ sample is shown on figure S7f. The Bi $4f_{5/2}$ and $4f_{7/2}$ peaks were found at binding energies of 165.9 eV and 160.4 eV, respectively. These binding energies are again slightly above those that would correspond to a Bi^{3+} state, indicating that the chemical environment seen by Bi 4f electrons when Bi replaces a Sb, resembles that of Bi^{5+}.
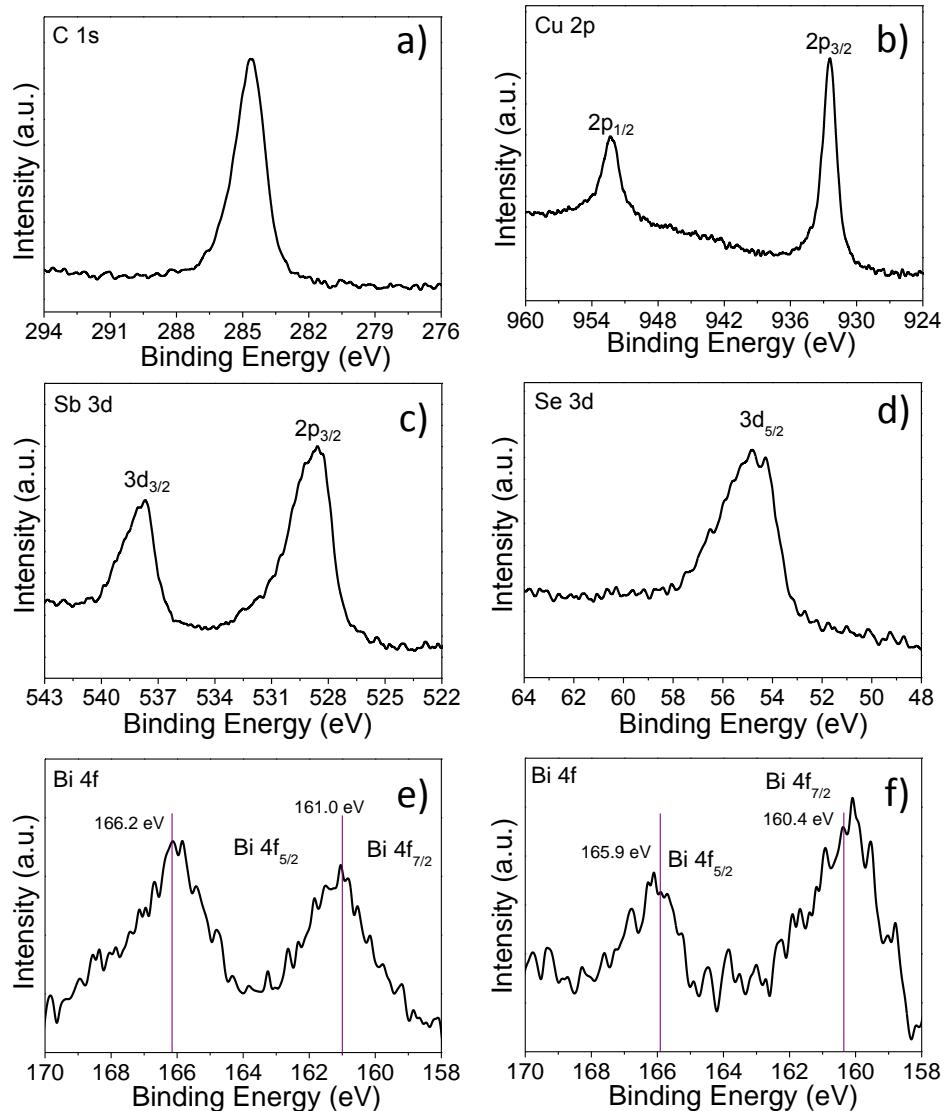
Figure S7. High resolution XPS spectrum of $Cu_3Sb_{0.90}Bi_{0.10}Se_4$ NCs and $Cu_3Sb_{0.88}Sn_{0.10}Bi_{0.02}Se_4$ NCs. a)-e) C 1s, Cu 2p, Sb 3d, Se 3d and Bi 4f spectra of $Cu_3Sb_{0.90}Bi_{0.10}Se_4$ NCs. f) Bi 4f spectra of $Cu_3Sb_{0.88}Sn_{0.10}Bi_{0.02}Se_4$ NCs.

6. TEM micrographs of Sn-, Bi- and Sn,Bi-doped CASe NCs
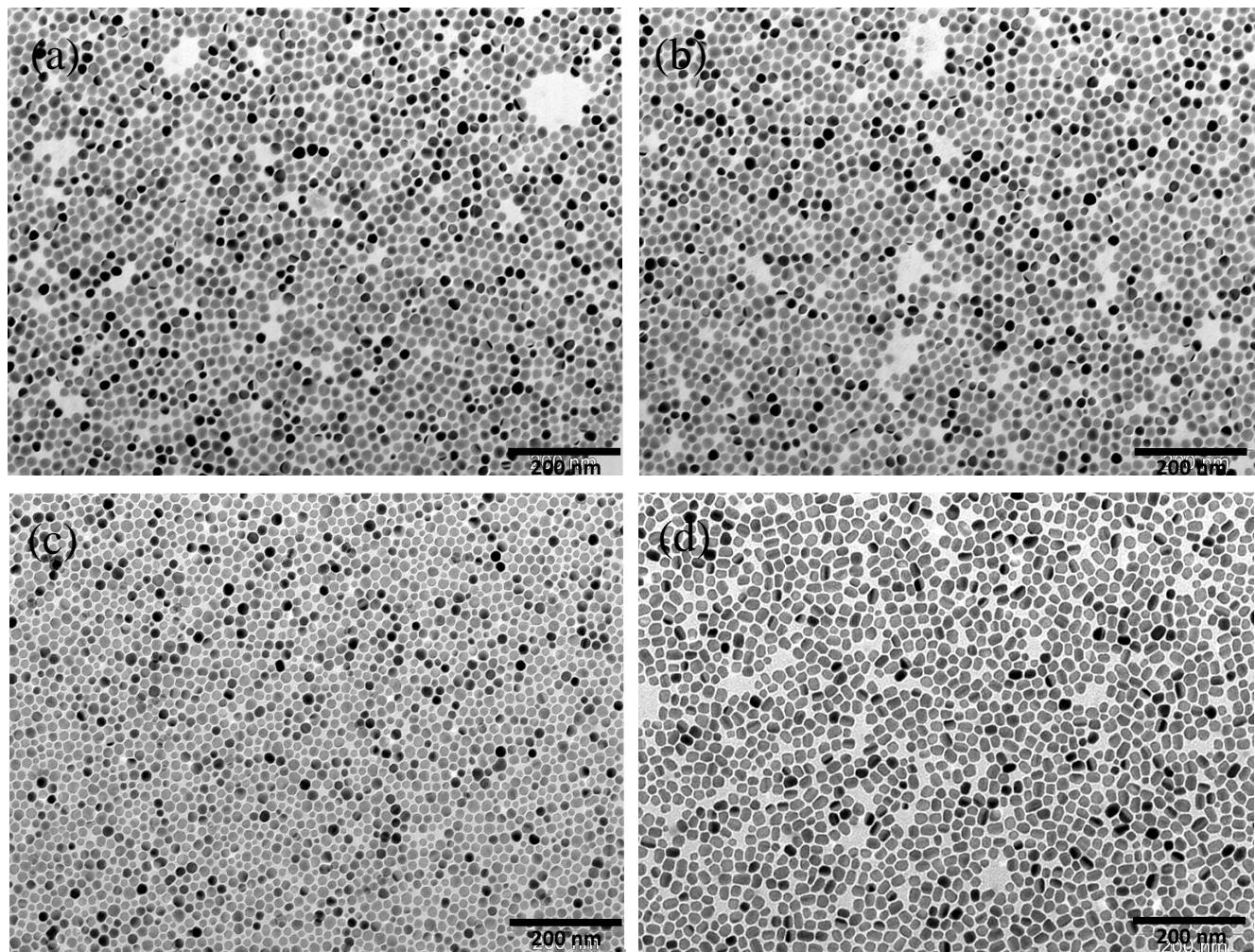
Figure S8. Representative TEM images of $Cu_3Sb_{1-x}Sn_xSe_4$ NCs with (a) x=0.01, (b) x=0.02, (c) x=0.05 and (d) x=0.10. Scale bars correspond to 200 nm.
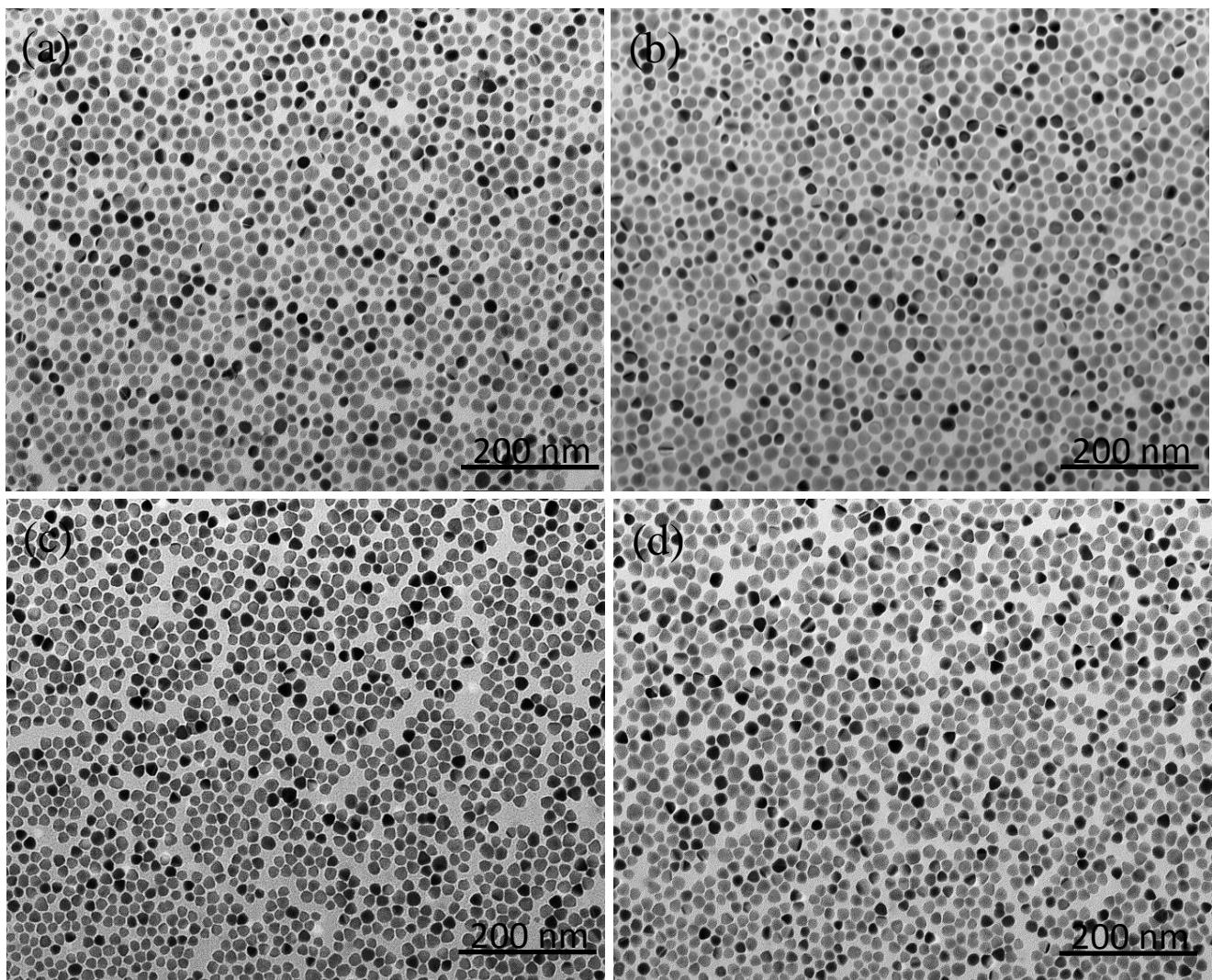
Figure S9. Representative TEM images of $Cu_3Sb_{1-x}Bi_xSe_4$ NCs with (a) x=0.01, (b) x=0.02, (c) x=0.04 and (d) x=0.10. Scale bars correspond to 200 nm.
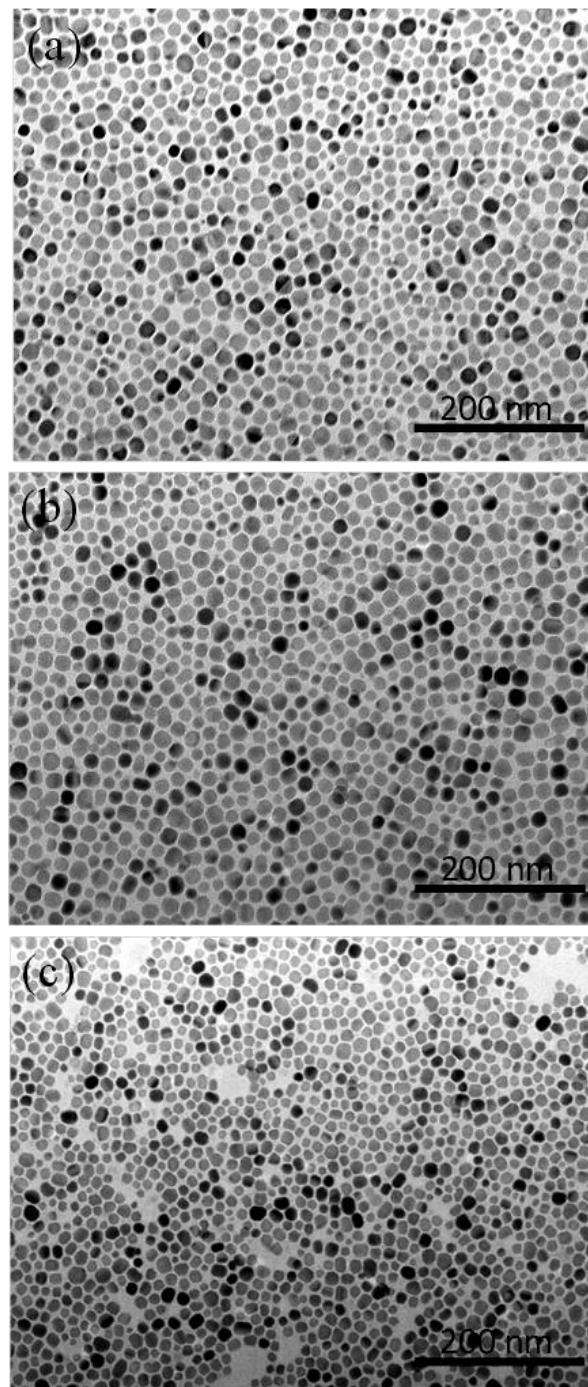
Figure S10. Representative TEM images of $Cu_3Sb_{0.98-x}Sn_xBi_{0.02}Se_4$ NCs with (a) x=0.02, (b) x=0.05 and (c) x=0.10. Scale bars correspond to 200 nm.

7. Composition of Sn- and Bi-doped CASe NCs
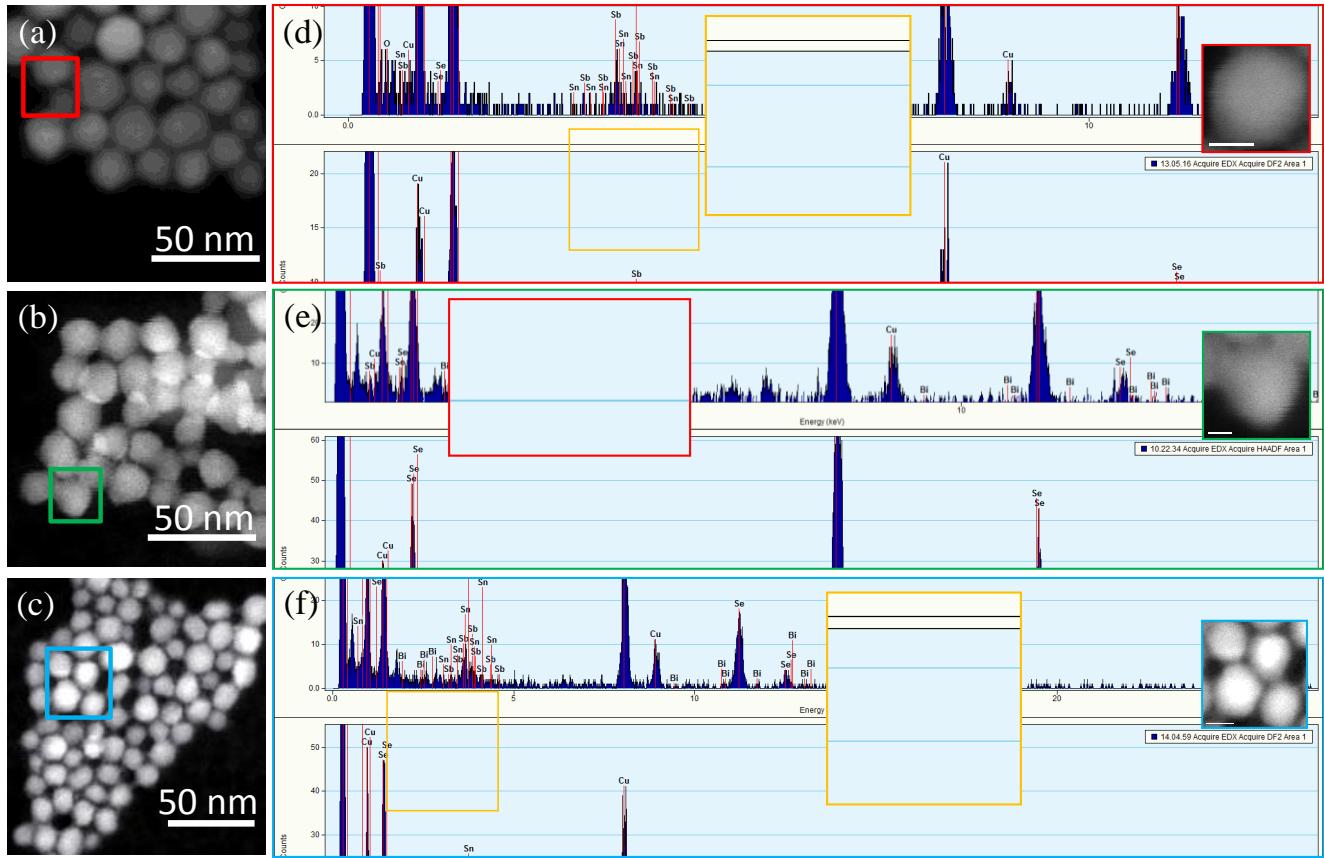
Figure S11. Left: ADF-STEM images of $Cu_3Sb_{0.98}Sn_{0.02}Se_4$ (a), $Cu_3Sb_{0.98}Bi_{0.02}Se_4$ (b) and $Cu_3Sb_{0.88}Sn_{0.10}Bi_{0.02}Se_4$ (c) NCs. Right: (d-f) EDX spectrum from single or few particles (inset), as indicated in the squared regions on the left. As observed, Sn and Sb peaks appear almost overlapped and the Sn signal was generally so weak that it was just on the detection threshold. Thus, although the analysis confirmed the presence of Sn, quantification was not possible. Similarly, the Bi signal could be observed in Bi-doped CASe, but it was quite weak, in the detection threshold, preventing quantification from single particle analysis.

(a)

Element	Wt%	At%
Cu	28.4	36.8
Sb	21.0	13.2
Sn	0.36	0.25
Se	50.2	49.7

$Cu_3Sb_{1.1}Sn_{0.02}Se_{4.1}$

(b)

Element	Wt%	At%
Cu	29.2	35.9
Sb	20.6	13.2
Bi	0.72	0.27
Se	49.4	50.5

$Cu_3Sb_{1.1}Bi_{0.02}Se_{4.1}$
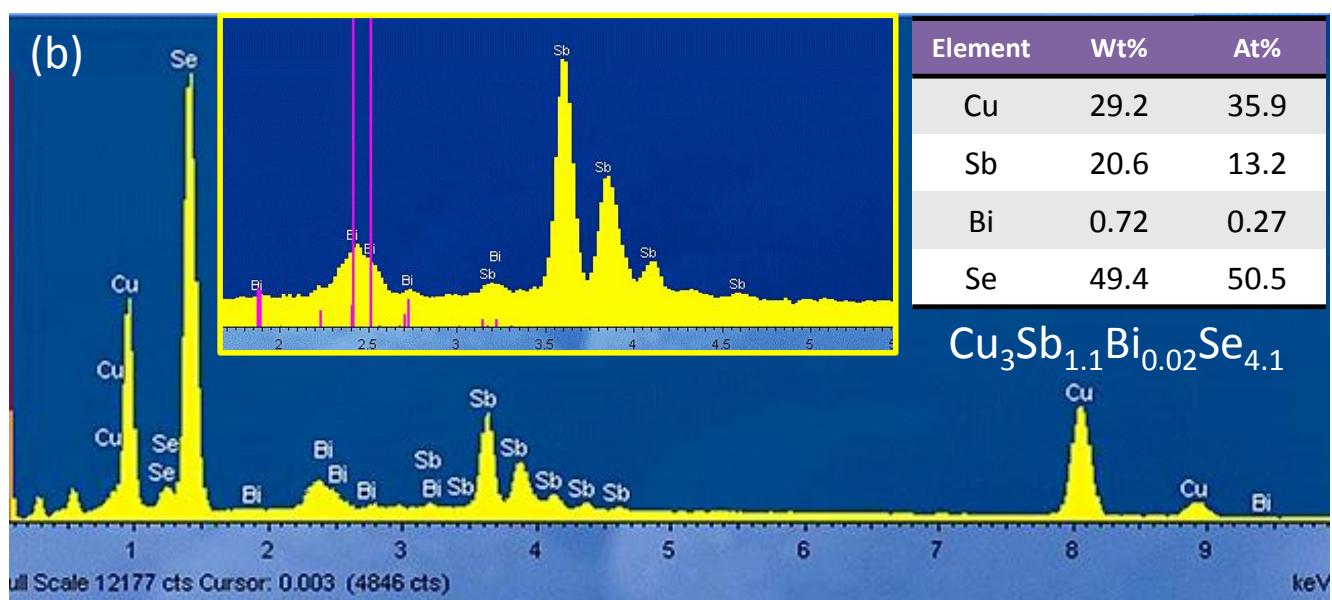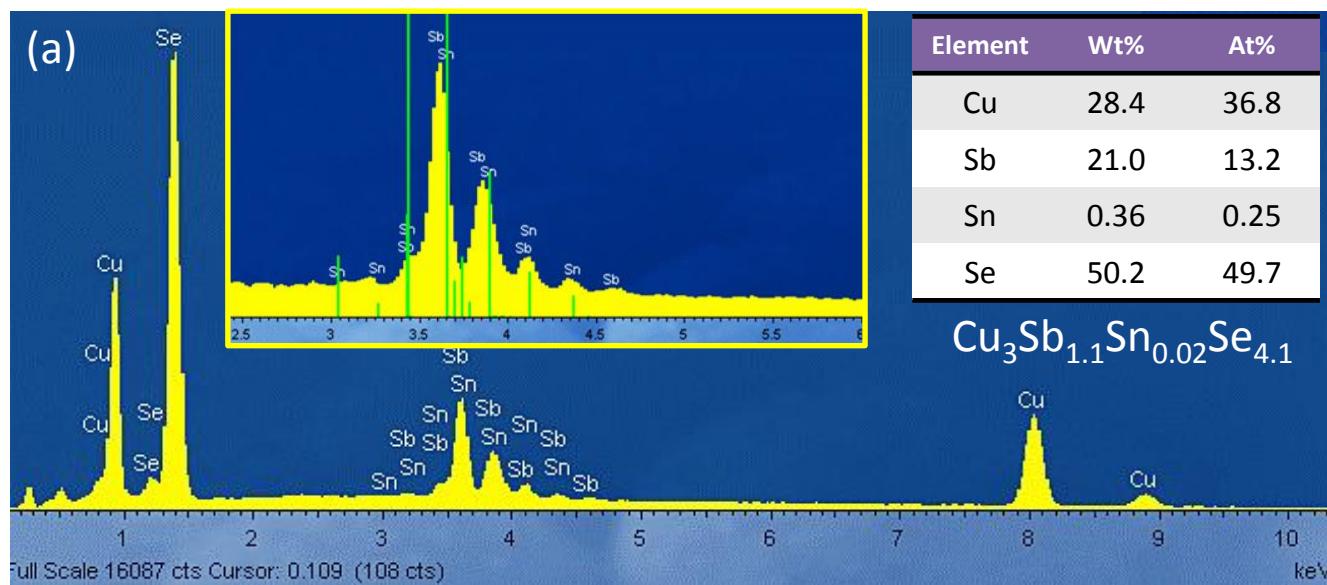
Figure S12. Representative SEM-EDX spectra of Sn-CASe and Bi-CASe consolidated materials.

Table S2. Composition of $Cu_3Sb_{1-x}Sn_xSe_4$ NCs obtained from ICP analysis.

Element	x=0	x=0.01	x=0.02	x=0.05	x=0.10
Cu	3	3	3	3	3
Sb	1.1	1.1	1.2	1.2	1.1
Sn	0	0.01	0.02	0.06	0.11

Table S3. Composition of $Cu_3Sb_{1-x}Bi_xSe_4$ NCs obtained from ICP analysis.

Element	x=0	x=0.02
Cu	3	3
Sb	1.1	1.1
Bi	0	0.02

Table S4. Composition of $Cu_3Sb_{1-x}Sn_xSe_4$ after consolidation obtained from SEM-EDX analysis.

Element	x=0.01	x=0.02	x=0.05	x=0.10
Cu	3.0	3.0	3.0	3.0
Sb	1.1	1.1	1.1	0.9
Sn	0.01	0.02	0.05	0.11
Se	3.8	4.1	4.0	3.9

Table S5. Composition of $Cu_3Sb_{1-x}Bi_xSe_4$ after consolidation obtained from SEM-EDX analysis.

Element	x=0.01	x=0.02	x=0.04	x=0.10
Cu	3.0	3.0	3.0	3.0
Sb	1.1	1.1	1.0	1.0
Bi	0.01	0.02	0.04	0.11
Se	3.9	4.1	3.7	4.0

Table S6. Composition of $Cu_3Sb_{1-x-y}Sn_xBi_ySe_4$ after consolidation obtained from SEM-EDX analysis.

Element	x=0.02, y=0.02	x=0.05, y=0.02	x=0.010, y=0.02
Cu	3.0	3.0	3.0
Sb	1.0	0.9	0.9
Sn	0.02	0.05	0.10
Bi	0.02	0.02	0.02
Se	3.8	3.9	3.9

8. Additional NMR data and FTIR spectra
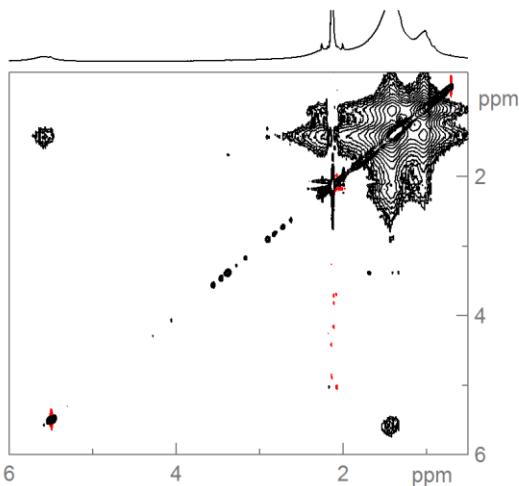
Figure S13. NOESY spectrum of CASe synthetized with OA.

Coefficient values ± one standard deviation	
A1	=1451.8 ± 50.1
D1	=45.236 ± 2.01
A2	=652.8 ± 98.4
D2	=551.97 ± 146
LD	=0.0025 ± 0
BD	=0.3 ± 0
S	=1 ± 0
ES	=0.6 ± 0
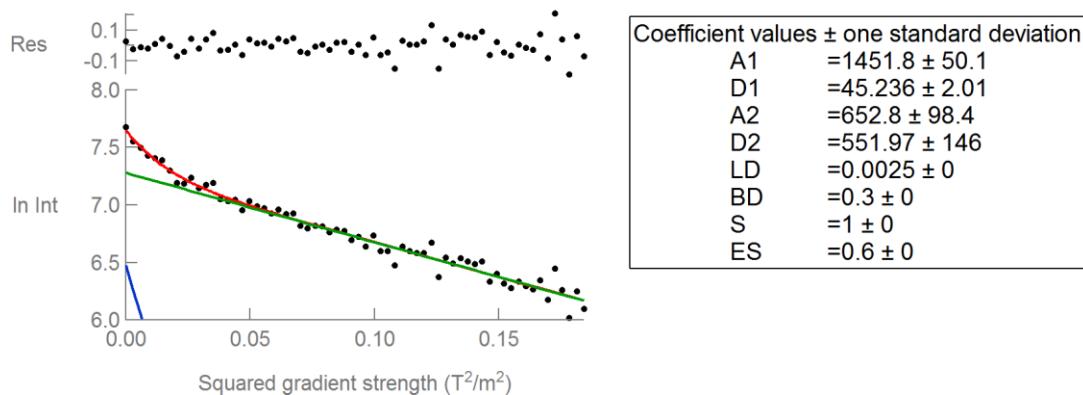
Figure S14. Fitting the signal intensity decay with the Stejskal-Tanner equation of CASe NPs synthetized with OA (further information on the experimental section). Bi exponential fitting with two different diffusion coefficients D1 and D2 (slow: 45 μm²/s => 16 nm; fast: 652 μm²/s).
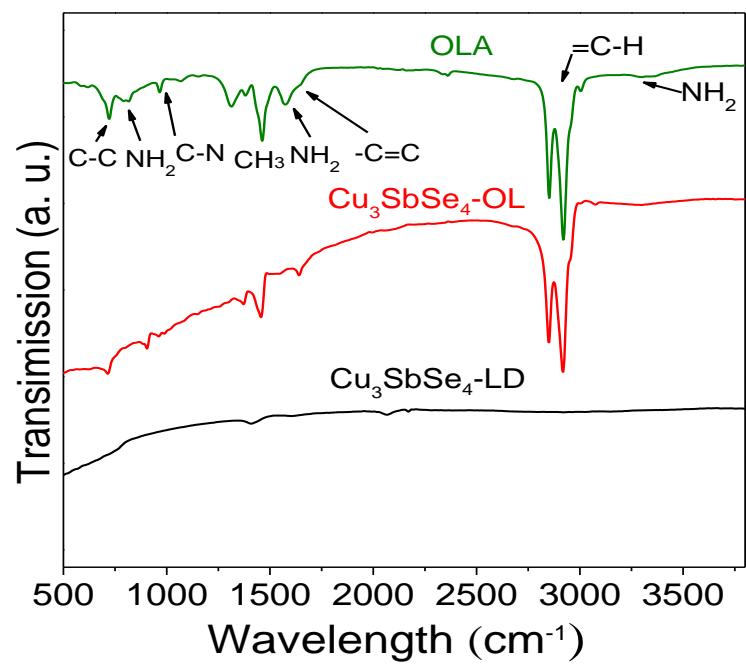
Figure S15. FTIR spectra of pure OLA, Cu_3SbSe_4–OL and Cu_3SbSe_4–LD NCs.

9. Pellet structural characterization
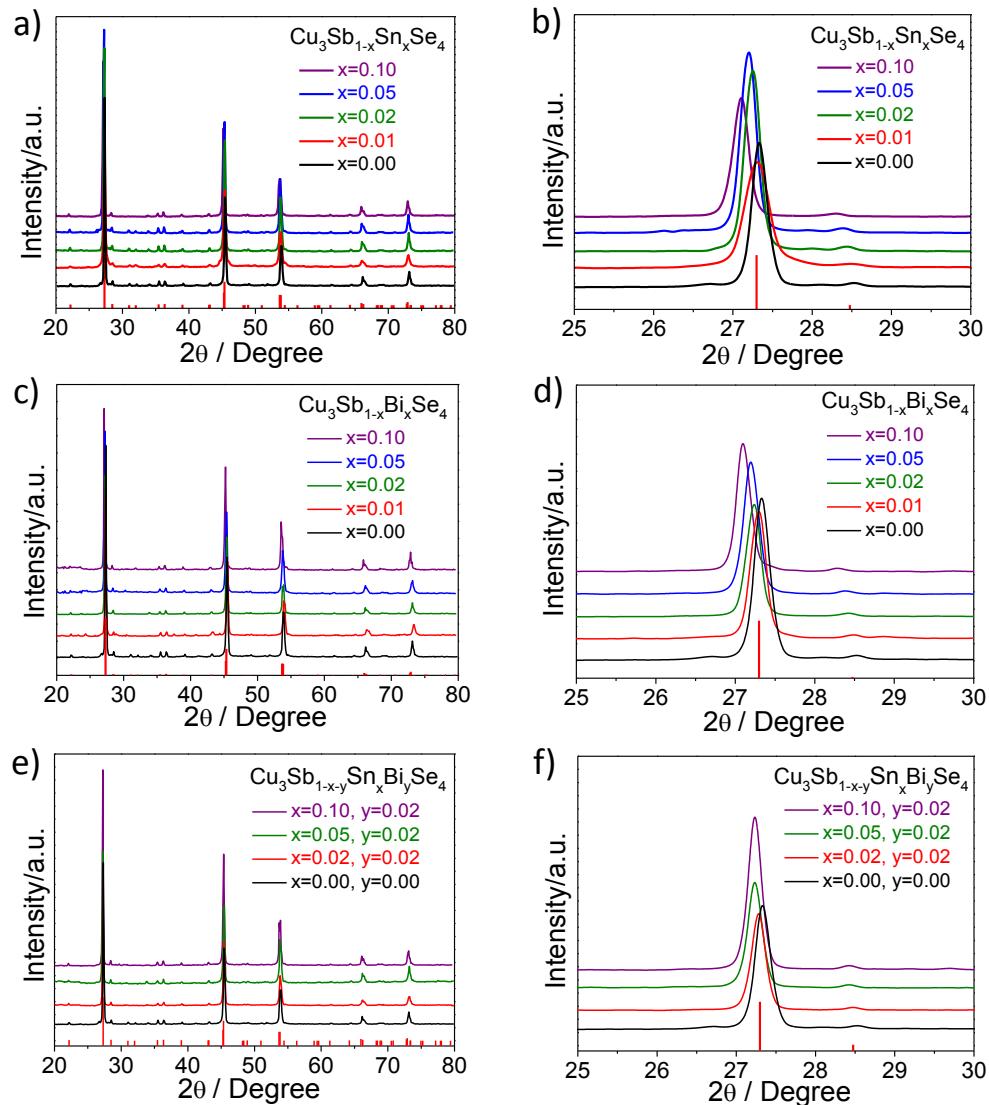
Figure S16. XRD patterns (a, c, e) and detail of the (112) peaks around 27.2° 2θ values (b, d, f) of a) $Cu_3Sb_{1-x}Sn_xSe_4$ (x=0.00, 0.01, 0.02, 0.05, 0.10), b) $Cu_3Sb_{1-x}Bi_xSe_4$ (x=0.00, 0.01, 0.02, 0.04, 0.10) and c) $Cu_3Sb_{1-x-y}Sn_xBi_ySe_4$ (x=0.02, 0.05, 0.10 and y=0.02) pellets. Red vertical lines correspond to the reference literature data for CASe, JCPDS NO. 85-0003.
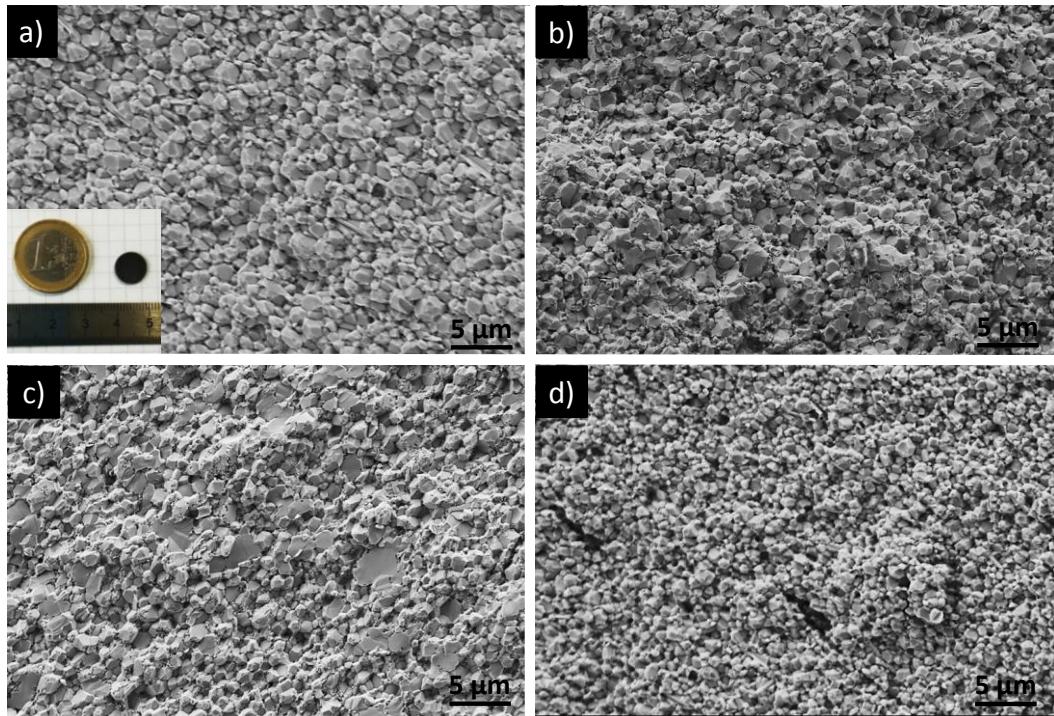
Figure S17. Representative SEM images of the fracture surfaces of bulk materials compacted from (a) Cu_3SbSe_4; (b) $Cu_3Sb_{0.98}Sn_{0.02}Se_4$; (c) $Cu_3Sb_{0.98}Bi_{0.02}Se_4$ and (d) $Cu_3Sb_{0.88}Sn_{0.10}Bi_{0.02}Se_4$ NCs. Inset of (a) shows one of the pellets measured.

10. Hall charge carrier concentrations and mobilities

Table S7. Room temperature carrier concentration (p), electrical conductivity (σ), and carrier mobility (μ) of Cu_3SbSe_4, $Cu_3Sb_{0.98}Sn_{0.02}Se_4$, $Cu_3Sb_{0.98}Bi_{0.02}Se_4$ and $Cu_3Sb_{0.88}Sn_{0.10}Bi_{0.02}Se_4$ samples.

Sample	p (cm^{-3})	σ (S cm^{-1})	μ (cm^{2}V^{-1}s^{-1})
Cu_3SbSe_4	5×10^{18}	29	36
$Cu_3Sb_{0.98}Sn_{0.02}Se_4$	9×10^{19}	454	32
$Cu_3Sb_{0.98}Bi_{0.02}Se_4$	2×10^{18}	26	58
$Cu_3Sb_{0.88}Sn_{0.10}Bi_{0.02}Se_4$	1×10^{20}	1309	80

11. Additional thermoelectric properties
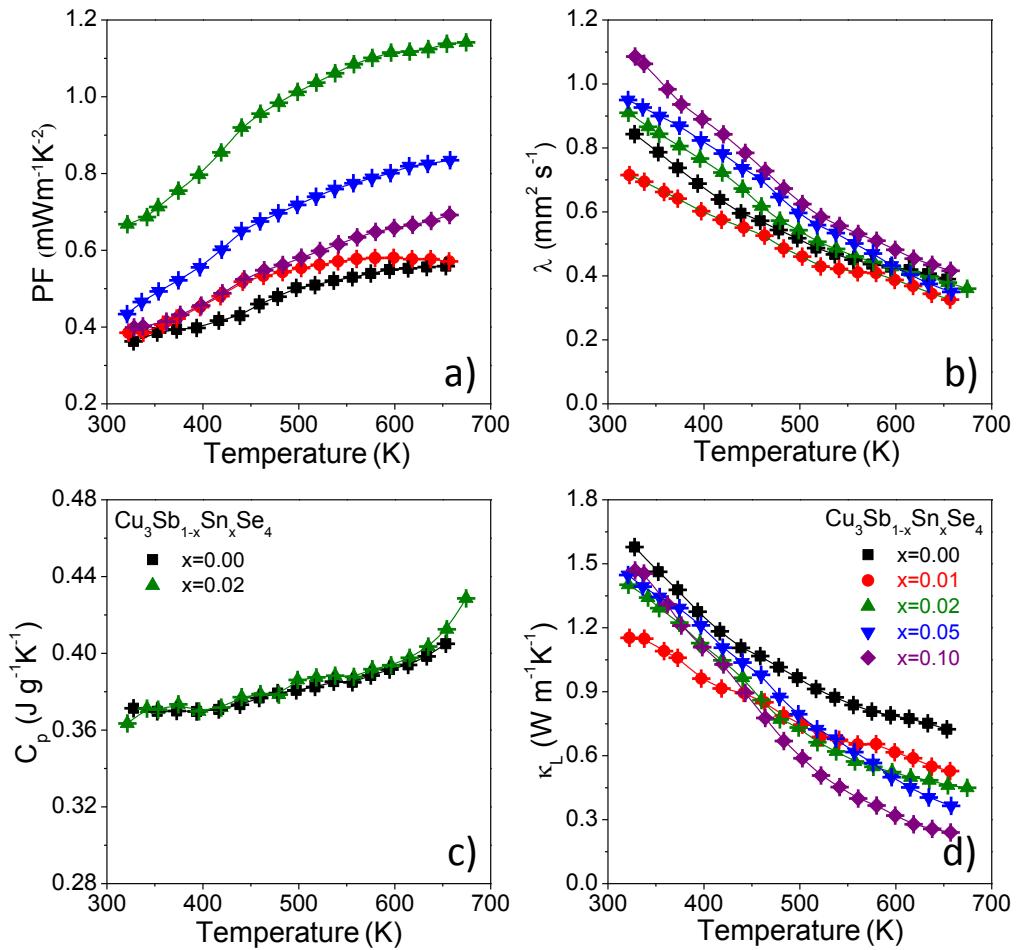
Figure S18. Temperature dependence of (a) power factor (PF), (b) thermal diffusivity (λ), (c) specific heat (C_p), and (d) lattice thermal conductivities (κ_L) of $Cu_3Sb_{1-x}Sn_xSe_4$ (x=0.01, 0.02, 0.05 and 0.10).
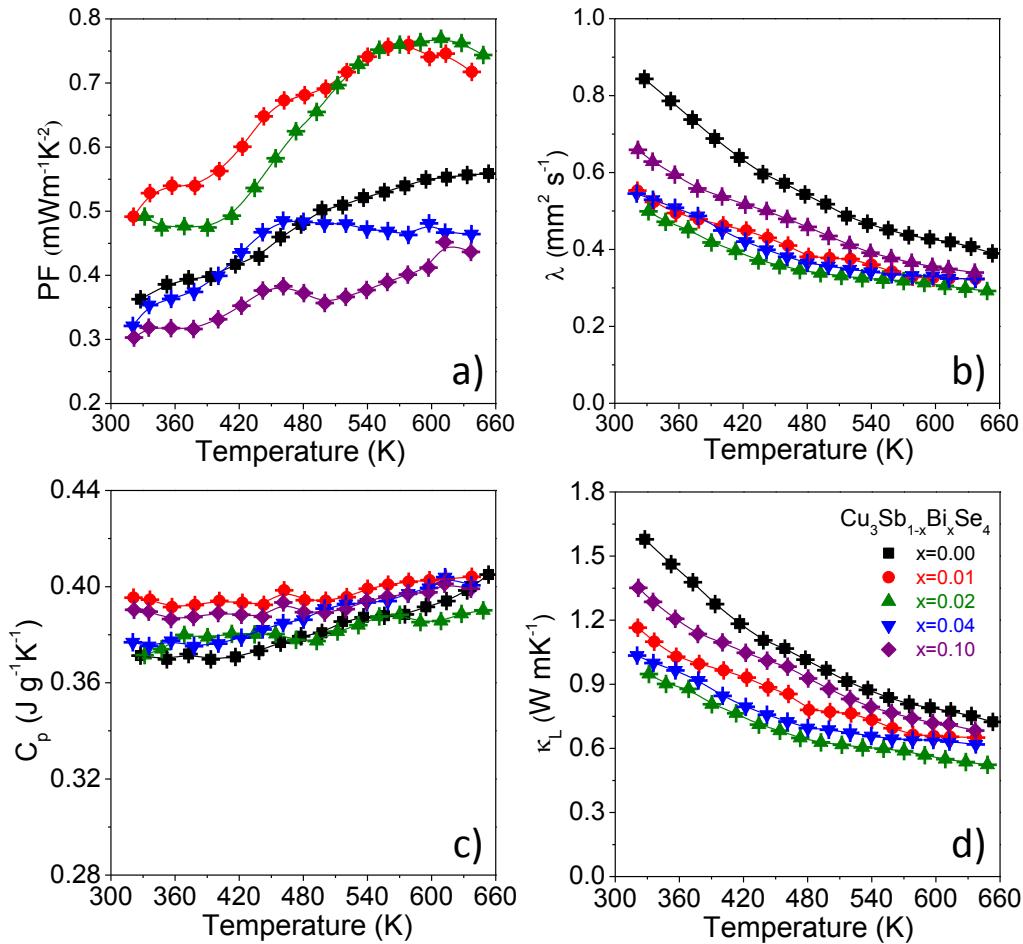
Figure S19. Temperature dependence of (a) power factor (PF), (b) thermal diffusivity (λ), (c) specific heat (C_p), and (d) lattice thermal conductivities (κ_L) of $Cu_3Sb_{1-x}Bi_xSe_4$ (x=0.01, 0.02, 0.04 and 0.10).
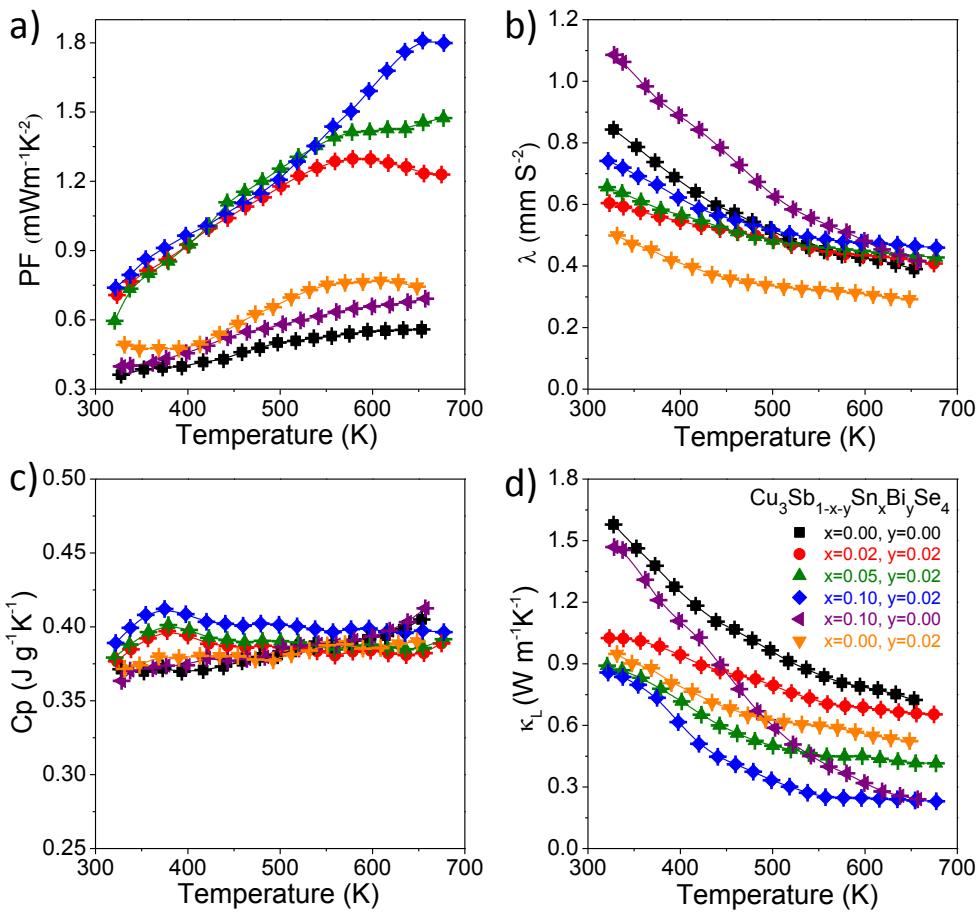
Figure S20. Temperature dependence of (a) power factor (PF), (b) thermal diffusivity (λ), (c) specific heat (C_p), and (d) lattice thermal conductivities (κ_L) of $Cu_3Sb_{1-x-y}Sn_xBi_ySe_4$ (x=0.01, 0.02, 0.05, 0.10 and y=0.02).

12. Stability

Samples were heated within the LINSEIS system in a He atmosphere up to 673 K at 10 K/min with the boron nitride coating before measurement. Such preliminary treatment warranted sample stability for all the cycles tested. All the samples were measured at least 3 consecutive times during heating up to around 673 K under the same conditions.
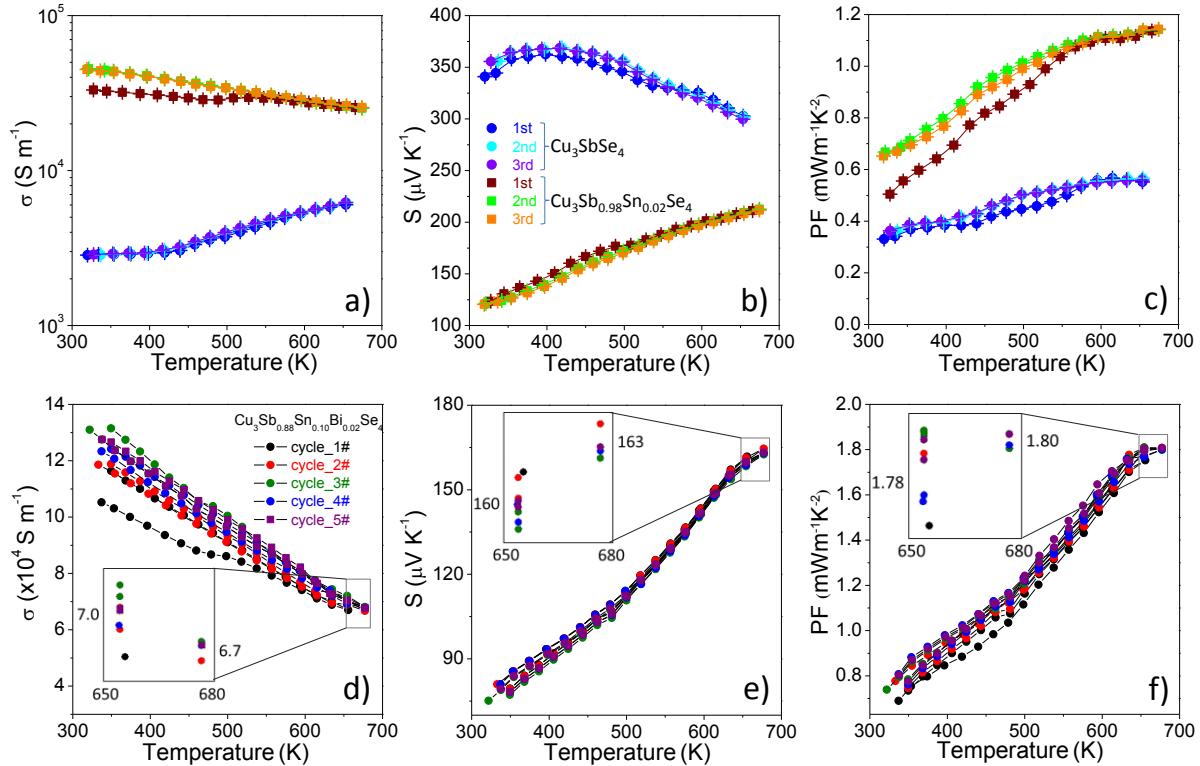
Figure S21. (a-c) Temperature dependence of the electrical conductivity (σ), Seebeck coefficient (S) and power factor (PF) of Cu_3SbSe_4 and $Cu_3Sb_{0.98}Sn_{0.02}Se_4$ measured 3 consecutive times during heating up to around 673 K. No pre-stabilization treatment was carried out before the first measurement. (d-f) display the thermoelectric properties of $Cu_3Sb_{0.88}Sn_{0.10}Bi_{0.02}Se_4$ pellet measured for 5 consecutive up-down cycles between room temperature and up to 673K. Measurements obtained during the first temperature ramp were slightly different from the ones obtained in posterior cycles, especially at low temperatures. We also observed a slight increase in electrical conductivity with the cycle number and no significant variation of the Seebeck coefficient in the low temperature range of the measurement.

13. DFT calculations

Table S8. Effective masses of studied compounds for holes (m^+) and electrons (m^-) along different directions of the Brillouin Zone. Effective masses are in unit of the mass electron (m_e).

		Γ-Z	Γ-X	Γ-A	Γ-M
CAse	m^-/m_e	0.06	0.17	0.19	0.18
	m^+/m_e	0.10	0.30	0.17	0.14
Bi-CASe	m^-/m_e	0.06	0.11	0.11	0.10
	m^+/m_e	0.10	0.32	0.20	0.15
Sn-CASe	m^-/m_e	0.07	0.13	0.14	0.13
	m^+/m_e	0.14	0.38	0.65	0.45
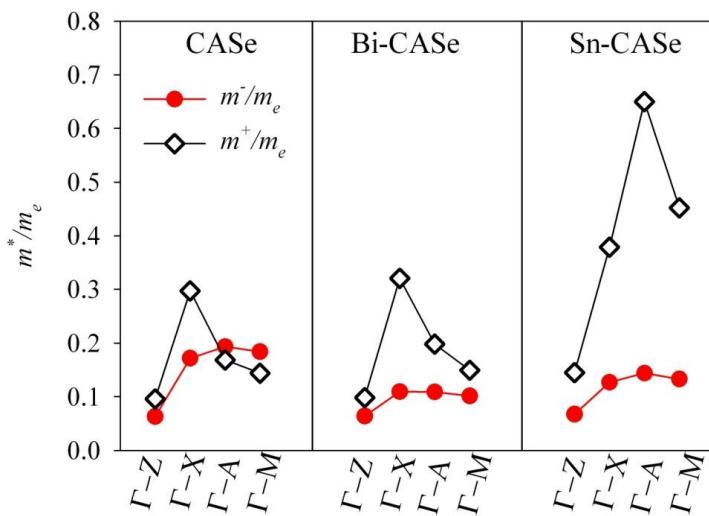
Figure S22. Effective masses for electrons (m$^-$) and holes (m$^+$) calculated from DFT for CASe, Bi-CASe and Sn-CASe

14. Influence of the minority carriers on the Seebeck coefficient

The measurement of the TE parameters from DFT calculations did not take into account the effect of the minority carriers. This effect becomes important as the temperature increases and more carriers of each type are thermally generated, eventually reaching densities comparable to that of the doping level.

To **qualitatively** determine the influence of the thermally generated charge carriers on the Seebeck coefficient, we calculated the Seebeck coefficient for holes and electrons using the expressions:

$$S_e = -\frac{8\pi^2 K_B^2}{3eh^2}\left(\frac{\pi}{3n}\right)^{2/3} m_e^* T \tag{1}$$

$$S_h = \frac{8\pi^2 K_B^2}{3eh^2}\left(\frac{\pi}{3p}\right)^{2/3} m_h^* T \tag{2}$$

Where K_B is the Boltzmann constant, e is the electron charge, h is the Plank constant and n, p, m_e^* and m_e^* are the charge carrier concentration and effective masses for electrons and holes.

We considered the following charge carrier concentrations:

$$n = n_i = \sqrt{M_c M_v}\, e^{-E_g/2K_B T} \tag{3}$$

$$p = p_0 + p_i = p_0 + n_i \tag{4}$$

Where n_i and p_i are the thermally generated charge carrier concentrations, p_0 is the hole concentration associated to the doping (which we consider independent of temperature) that we could approximate to the value measured at ambient temperature by Hall effect, E_g is the semiconductor band gap and M_c and M_v are the densities of states at the CBM and VBM, respectively. We approximate the values of M_c and M_v to:

$$M_c = 2\left(\frac{2\pi m_e^* K_B T}{h^2}\right)^{3/2} \tag{5}$$

$$M_v = 2\left(\frac{2\pi m_h^* K_B T}{h^2}\right)^{3/2} \tag{6}$$

Then we calculate the Seebeck coefficient using:

$$S = \frac{S_n \sigma_n + S_p \sigma_p}{\sigma_n + \sigma_p} \tag{7}$$

with

$$\sigma_n = en\mu_n \tag{8}$$

$$\sigma_p = ep\mu_p \tag{9}$$

In our calculations, we took: $\mu_n = 2\mu_p$ and used the values of E_g, m_e^* and m_h^* obtained from DFT calculations. Overall this calculation cannot be used to obtain a quantitative fitting to the experimental data due to the many approximations used. However we believe it gives a useful qualitative view of the influence of the thermally generated carriers on the Seebeck coefficient.
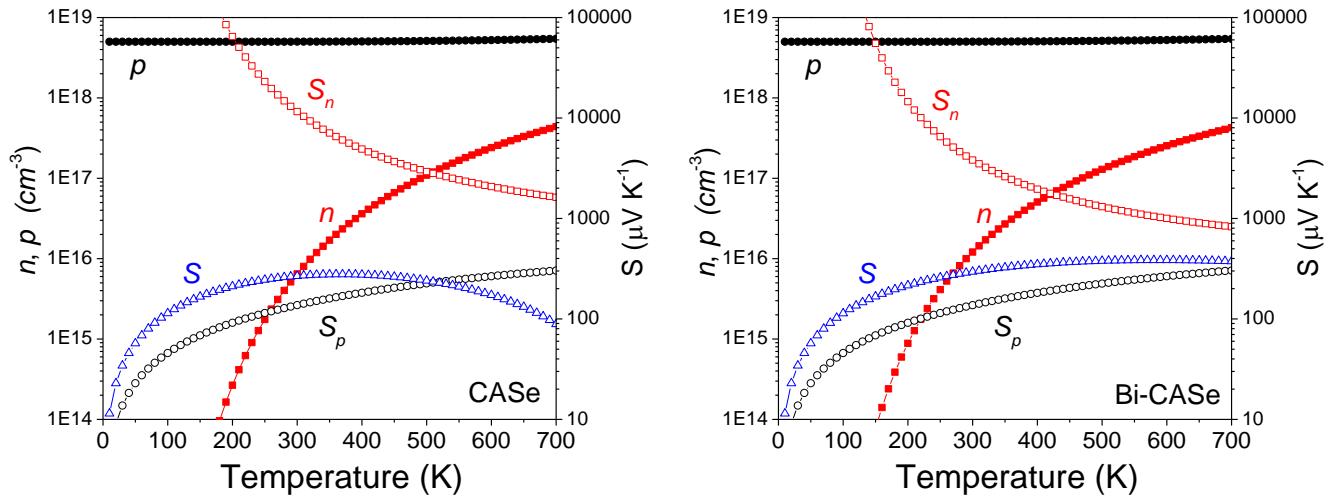
Figure S23. Temperature dependence of the charge carrier concentrations (n, p) and Seebeck coefficients (Sn, Sp, S) of Cu_3SbSe_4 (left) and $Cu_3Sb_{0.875}Bi_{0.125}Se_4$ (right) calculated using equations 1-7 and considering $p_0 = 5 \times 10^{18}$.

Notice how in spite of the lower bandgap of Bi-CASe, and thus the higher charge carrier concentrations associated to thermal generation, the reduced m_e^* in this compound translates in a lower S_n and thus an overall higher Seebeck coefficient.

It should be noticed that the introduction of Sn also translates into larger differences in the effective masses of holes and electrons and that in spite of the strong band gap decrease in this material, the calculated Seebeck coefficients at moderate doping concentrations are higher than those of CASe and even Bi-CASe. However, the introduction of sufficient amounts of Sn to modify the band structure has associated the injection of very large amounts of charge carrier, which inevitably results in overall lower Seebeck coefficients. Thus the introduction of both dopants, Sn to control charge carrier concentration and Bi to modify the band structure is necessary to optimize performance in this material.
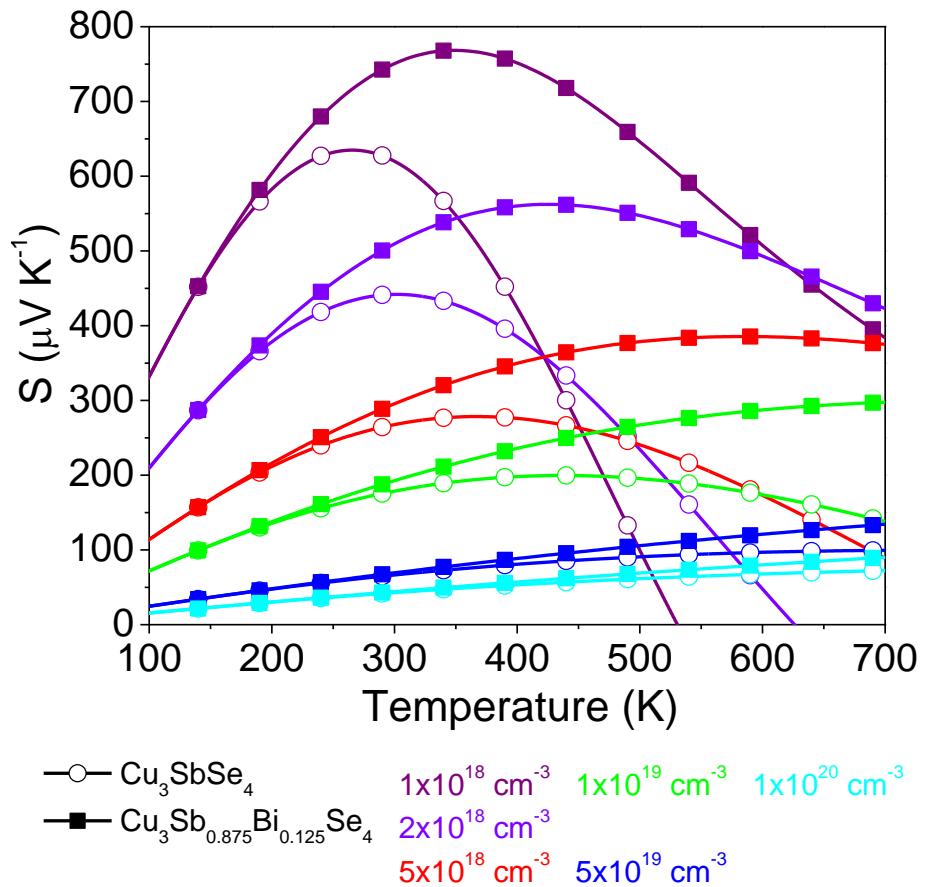
Figure S24. Temperature dependence of the Seebeck coefficient (S) of Cu_3SbSe_4 and $Cu_3Sb_{0.875}Bi_{0.125}Se_4$ calculated using equation 1-9 for different doping levels as indicated by the different colors.

15. TE properties literature comparison

Table S9. State-of-art thermoelectric performance values for Pb- and Te-free Cu- and Ag-based chalcogenides and some other Pb- and Te- free compounds at 673 K (excepted when otherwise specified).

Material	σ, x10^3 Sm^{-1}	S, μV/K	PF, mWm^{-1}K^{-2}	κ, Wm^{-1}K^{-1}	ZT	Ref.
$Cu_{0.975}BiSeO$	3.2	230	0.17	0.50	0.23	[12]
Cu_2GeSe_3	5.2	160	0.13	0.39	0.23	[13]
$CuFeS_2$	0.33	816	0.23	0.43	0.26 (500 K)	[14]
Cu_2SnSe_3	6.0	215	0.28	0.68	0.27	[15]
Cu_2SnSe_3	12	299	1.07	1.91	0.34 (598 K)	[16]
$Cu_{2.15}Zn_{0.85}GeSe_{3.9}$	25	100	0.25	0.41	0.41	[17]
$Cu_2Sn_{0.90}In_{0.10}Se_3$	49	150	1.10	1.52	0.49	[18]
$Cu_3Sb_{0.98}Sn_{0.02}Se_4$	24	200	0.96	1.10	0.50 (575 K)	[19]
$Cu_2CdSnSe_4$	24	170	0.70	0.85	0.55	[20]
$AgBiSe_{1.98}Cl_{0.02}$	21	-150	0.47	0.56	0.56	[21]
$Cu_3Sb_{0.97}Al_{0.03}Se_4$	20	230	1.05	1.08	0.58 (600 K)	[22]
$Cu_{2.15}Cd_{0.85}SnSe_{3.9}$	7.9	165	0.22	0.25	0.59	[23]
$Cu_{2.1}Cd_{0.9}SnSe_4$	20	155	0.48	0.55	0.59	[24]
$Cu_{1.85}Ag_{0.15}Sn_{0.85}In_{0.15}Se_3$	46	140	0.90	1.01	0.60	[25]
$Cu_2Sn_{0.90}In_{0.10}Se_3$	50	150	1.13	1.12	0.68	[26]
$CuBi_{0.875}Ba_{0.125}SeO$	24	152	0.56	0.55	0.69	[27]
$Cu_3Sb_{0.98}Bi_{0.02}Se_4$	10	325	1.10	0.90	0.70 (600 K)	[28]
$AgSb_{0.96}Pb_{0.04}Se_2$	2.3	375	0.32	0.30	0.70	[29]
$Cu_3Sb_{0.975}Sn_{0.025}Se_4$	23	235	1.30	1.17	0.75	[30]
$Ag_{0.96}Nb_{0.04}BiSe_2$	19	-200	0.76	0.64	0.80	[31]
β-Cu_2Se	24	210	1.07	0.90	0.80	[32]
β-Zn_4Sb_3	33	183	1.09	0.75	0.80 (550 K)	[33]
$Cu_3Sb_{0.97}Ge_{0.03}Se_{2.8}S_{1.2}$	22	235	1.20	0.91	0.89 (650 K)	[34]
$CuAgSe$	10	202	0.41	0.28	0.90 (623 K)	[35]
$Cu_{1.97}S$	16	210	0.70	0.52	0.91	[36]
$AgSb_{0.99}Na_{0.01}Se_2$	4.4	340	0.51	0.37	0.92	[37]
$Cu_3Sb_{0.98}Sn_{0.02}Se_4$	29	230	1.55	1.10	0.95	[38]
$AgSb_{0.98}Ba_{0.02}Se_2$	4.2	350	0.51	0.35	0.98	[39]
$AgSb_{0.98}Cd_{0.02}Se_2$	5.4	325	0.57	0.37	0.98 (640 K)	[40]
$Ag_2Se_{1.08}$	20	-125	0.32	1.30	0.99 (400 K)	[41]
$AgSb_{0.98}Mg_{0.02}Se_2$	6.7	300	0.60	0.40	1.00	[39]
$AgSbSe_2$–$ZnSe$	5.0	348	0.60	0.40	1.00	[42]
$Mm_{0.9}Fe_{3.1}Co_{0.9}Sb_{12}$	75	202	3.06	1.96	1.05	[43]

$AgBi_{0.5}Sb_{0.5}Se_2$	3.3	275	0.25	0.13	1.07 (550 K)	[44]
$YbCd_{1.9}Mg_{0.1}Sb_2$	32	230	1.70	1.03	1.08 (650K)	[45]
$AgSb_{0.98}Bi_{0.02}Se_2$	5.3	330	0.58	0.35	1.10	[29]
$In_{0.27}Co_4Sb_{11.9}$	80	-225	4.06	2.5	1.13	[46]
$Cu_{11}MnSb_4S_{13}$	28	145	0.58	0.29	1.13 (575 K)	[47]
$In_{0.2}Co_4Sb_{12}$	63	-245	3.77	1.95	1.20(620 K)	[48]
$In_{0.2}Ce_{0.05}Yb_{0.1}Co_4Sb_{12}$	44	-252	2.81	1.45	1.20 (620 K)	[48]
$In_{0.25}Co_4Sb_{12}$	62	-270	4.53	2.17	1.20 (575 K)	[49]
$AgSb_{0.99}Sn_{0.01}Se_2$	9.2	295	0.80	0.44	1.21 (660 K)	[50]
$AgBiSe_2$	2.3	450	0.47	0.25	1.25	[51]
$Cu_3Sb_{0.88}Sn_{0.10}Bi_{0.02}Se_4$	68	163	1.80	0.97	1.26	This work
$In_{0.2}Ce_{0.15}Co_4Sb_{12}$	63	-240	3.65	1.63	1.40 (625 K)	[48]
$(Zr_{0.5}Hf_{0.5})_{0.5}Ti_{0.5}Ni$ $Sn_{0.998}Sb_{0.002}$	68	-300	6.14	2.85	1.45	[52]
$Ti_{0.5}(Zr_{0.5}Hf_{0.5})_{0.5}Ni$ $Sn_{0.998}Sb_{0.002}$	65	-310	6.25	2.90	1.45	[53]
$SnSe$	30	280	2.35	0.75	2.0	[54]

16. References

1. S. Li, Z. Zhao, Q. Liu, L. Huang, G. Wang, D. Pan, H. Zhang and X. He, *Inorg. Chem.*, 2011, **50**, 11958-11964.
2. v. NIST-XPS database, http://srdata.nist.gov/xps/, accessed Nov 30, 2011.
3. L. Partain, R. Schneider, L. Donaghey and P. Mcleod, *J. Appl. Phys.*, 1985, **57**, 5056-5065.
4. D. Do, V. Ozolins, S. D. Mahanti, M. S. Lee, Y. Zhang and C. Wolverton, *J. Phys. Condens. Matter*, 2012, **24**, 415502.
5. E. J. Skoug and D. T. Morelli, *Phys. Rev. Lett.*, 2011, **107**, 235901.
6. T.-R. Wei, H. Wang, Z. M. Gibbs, C.-F. Wu, G. J. Snyder and J.-F. Li, *J. Mater. Chem. A,* 2014, **2**, 13527-13533.
7. M.-Y. Chiang, S.-H. Chang, C.-Y. Chen, F.-W. Yuan and H.-Y. Tuan, *J. Phys. Chem. C,* 2011, **115**, 1592-1599.
8. A. Politano, M. Caputo, S. Nappini, F. Bondino, E. Magnano, Z. Aliev, M. Babanly, A. Goldoni, G. Chiarello and E. Chulkov, *J. Phys. Chem. C*, 2014, **118**, 21517-21522.
9. V. Nascimento, V. De Carvalho, R. Paniago, E. Soares, L. Ladeira and H. Pfannes, *J. Electron. Spectrosc. Relat. Phenom.*, 1999, **104**, 99-107.
10. L. Song, S. Zhang, C. Chen, X. Hu and Q. Wei, *Chem. Eng. J.*, 2011, **171**, 1454-1457.
11. J. F. Moulder, W. F. Stickle, P. E. Sobol and K. D. Bomben, *Handbook of X-ray Photoelectron Spectroscopy: A Reference Book of Standard Spectra for Identification and Interpretation of XPS Data*, Physical Electronics Division, Perkin-Elmer Corporation, 2nd ed. edn., 1992.
12. Y. Liu, L.-D. Zhao, Y. Liu, J. Lan, W. Xu, F. Li, B.-P. Zhang, D. Berardan, N. Dragoe and Y.-H. Lin, *J. Am. Chem. Soc.*, 2011, **133**, 20112-20115.
13. M. Ibáñez, R. Zamani, W. Li, D. Cadavid, S. p. Gorsse, N. A. Katcho, A. Shavel, A. M. López, J. R. Morante, J. Arbiol and A. Cabot, *Chem. Mater.*, 2012, **24**, 4615-4622.
14. D. Liang, R. Ma, S. Jiao, G. Pang and S. Feng, *Nanoscale*, 2012, **4**, 6265-6268.
15. M. Ibáñez, D. Cadavid, U. Anselmi-Tamburini, R. Zamani, S. Gorsse, W. Li, A. M. López, J. R. Morante, J. Arbiol and A. Cabot, *J. Mater. Chem. A*, 2013, **1**, 1421-1426.
16. J.-M. Song, Y. Liu, H.-L. Niu, C.-J. Mao, L.-J. Cheng, S.-Y. Zhang and Y.-H. Shen, *J. Alloys Compd.*, 2013, **581**, 646-652.
17. M. Ibáñez, R. Zamani, A. LaLonde, D. Cadavid, W. Li, A. Shavel, J. Arbiol, J. R. Morante, S. Gorsse, G. J. Snyder and A. Cabot, *J. Am. Chem. Soc.*, 2012, **134**, 4060-4063.
18. X. Shi, L. Xi, J. Fan, W. Zhang and L. Chen, *Chem. Mater.*, 2010, **22**, 6029-6031.
19. Y. Wu, X. Qiao, X. Fan, X. Zhang, S. Cui and J. Wan, *J. Nanopart. Res.*, 2015, **17**, 1-7.
20. F.-J. Fan, B. Yu, Y.-X. Wang, Y.-L. Zhu, X.-J. Liu, S.-H. Yu and Z. Ren, *J. Am. Chem. Soc.*, 2011, **133**, 15910-15913.
21. S. N. Guin, V. Srihari and K. Biswas, *J. Mater. Chem. A*, 2015, **3**, 648-655.
22. Y. Li, X. Qin, D. Li, X. Li, Y. Liu, J. Zhang, C. Song and H. Xin, *Rsc Adv.*, 2015, **5**, 31399-31403.
23. M. Ibáñez, D. Cadavid, R. Zamani, N. García-Castelló, V. Izquierdo-Roca, W. Li, A. Fairbrother, J. D. Prades, A. Shavel, J. Arbiol, A. Pérez-Rodríguez, J. R. Morante and A. Cabot, *Chem. Mater.*, 2012, **24**, 562-570.
24. M. L. Liu, I. W. Chen, F. Q. Huang and L. D. Chen, *Adv. Mater.*, 2009, **21**, 3808-3812.
25. Y. Li, G. Liu, T. Cao, L. Liu, J. Li, K. Chen, L. Li, Y. Han and M. Zhou, *Adv. Funct. Mater.*, 2016.
26. Y. Li, G. Liu, J. Li, K. Chen, L. Li, Y. Han, M. Zhou, M. Xia, X. Jiang and Z. Lin, *New J. Chem.*, 2016.
27. J. Li, J. Sui, Y. Pei, C. Barreteau, D. Berardan, N. Dragoe, W. Cai, J. He and L.-D. Zhao, *Energy Environ. Sci.,* 2012, **5**, 8543-8547.
28. X. Li, D. Li, H. Xin, J. Zhang, C. Song and X. Qin, *J. Alloys Compd.*, 2013, **561**, 105-108.
29. S. N. Guin, A. Chatterjee, D. S. Negi, R. Datta and K. Biswas, *Energy Environ. Sci.,* 2013, **6**, 2603-2608.
30. C. Yang, F. Huang, L. Wu and K. Xu, *J. Phys. D: Appl. Phys.*, 2011, **44**, 295404.
31. L. Pan, D. Bérardan and N. Dragoe, *J. Am. Chem. Soc.*, 2013, **135**, 4914-4917.
32. H. Liu, X. Shi, F. Xu, L. Zhang, W. Zhang, L. Chen, Q. Li, C. Uher, T. Day and G. J. Snyder, *Nat. Mater.*, 2012, **11**, 422-425.
33. E. S. Toberer, P. Rauwel, S. Gariel, J. Taftø and G. J. Snyder, *J. Mater. Chem.*, 2010, **20**, 9877-9885.
34. E. J. Skoug, J. D. Cain and D. T. Morelli, *Appl. Phys. Lett.*, 2011, **98**, 261911.
35. C. Han, Q. Sun, Z. X. Cheng, J. L. Wang, Z. Li, G. Q. Lu and S. X. Dou, *J. Am. Chem. Soc.*, 2014, **136**, 17626-17633.
36. Y. He, T. Day, T. Zhang, H. Liu, X. Shi, L. Chen and G. J. Snyder, *Adv. Mater.*, 2014, **26**, 3974-3978.
37. S. Cai, Z. Liu, J. Sun, R. Li, W. Fei and J. Sui, *Dalton Trans.*, 2015, **44**, 1046-1051.
38. D. Li, R. Li, X.-Y. Qin, C.-J. Song, H.-X. Xin, L. Wang, J. Zhang, G.-l. Guo, T.-H. Zou and Y.-F. Liu, *Dalton*

Trans., 2014, **43**, 1888-1896.

39. Z. Liu, J. Shuai, H. Geng, J. Mao, Y. Feng, X. Zhao, X. Meng, R. He, W. Cai and J. Sui, *ACS Appl. Mater. Interfaces,* 2015, **7**, 23047-23055.
40. S. N. Guin, A. Chatterjee and K. Biswas, *RSC Adv.*, 2014, **4**, 11811-11815.
41. W. Mi, P. Qiu, T. Zhang, Y. Lv, X. Shi and L. Chen, *Appl. Phys. Lett.*, 2014, **104**, 133903.
42. S. N. Guin, D. S. Negi, R. Datta and K. Biswas, *J. Mater. Chem. A*, 2014, **2**, 4324-4331.
43. T. Dahal, S. Gahlawat, Q. Jie, K. Dahal, Y. Lan, K. White and Z. Ren, *J. Appl. Phys.*, 2015, **117**, 055101.
44. C. Xiao, J. Xu, B. Cao, K. Li, M. Kong and Y. Xie, *J. Am. Chem. Soc.*, 2012, **134**, 7971-7977.
45. Q. Cao, J. Zheng, K. Zhang and G. Ma, *J. Alloys Compd.*, 2016, **680**, 278-282.
46. Y. Tang, Y. Qiu, L. Xi, X. Shi, W. Zhang, L. Chen, S.-M. Tseng, S.-w. Chen and G. J. Snyder, *Energy Environ. Sci.,* 2014, **7**, 812-819.
47. J. Heo, G. Laurita, S. Muir, M. A. Subramanian and D. A. Keszler, *Chem. Mater.*, 2014, **26**, 2047-2051.
48. K. Biswas, M. S. Good, K. C. Roberts, M. Subramanian and T. J. Hendricks, *J. Mater. Res.*, 2011, **26**, 1827-1835.
49. T. He, J. Chen, H. D. Rosenfeld and M. Subramanian, *Chem. Mater.*, 2006, **18**, 759-762.
50. D. Li, X. Qin, T. Zou, J. Zhang, B. Ren, C. Song, Y. Liu, L. Wang, H. Xin and J. Li, *J. Alloys Compd.*, 2015, **635**, 87-91.
51. C. Xiao, X. Qin, J. Zhang, R. An, J. Xu, K. Li, B. Cao, J. Yang, B. Ye and Y. Xie, *J. Am. Chem. Soc.*, 2012, **134**, 18460-18466.
52. S. Sakurada and N. Shutoh, *Appl. Phys. Lett.*, 2005, **86**, 082105.
53. N. Shutoh and S. Sakurada, *J. Alloys Compd.*, 2005, **389**, 204-208.
54. L.-D. Zhao, G. Tan, S. Hao, J. He, Y. Pei, H. Chi, H. Wang, S. Gong, H. Xu and V. P. Dravid, *Science*, 2016, **351**, 141-144.